NVU view on energy polydisperse Lennard-Jones systems

Danqi Lang, Lorenzo Costigliola, and Jeppe C. Dyre*
Glass and Time, IMFUFA, Department of Science and Environment, Roskilde University, P.O. Box 260, DK-4000 Roskilde, Denmark
(Dated: November 13, 2024)

Lennard-Jones (LJ) systems exhibit strikingly invariant structure and dynamics when energy polydispersity is introduced [Ingebrigtsen and Dyre, J. Phys. Chem. B **127**, 2837 (2023)]. For instance, at a given state point the radial distribution function and the mean-square displacement as a function of time are virtually unaffected by energy polydispersity, which is in contrast to what happens when size polydispersity is introduced. We here argue – and validate by simulations of up to 30% polydispersity – that this invariance reflects an approximate invariance of the constant-potential-energy hypersurface. NVU dynamics is defined as geodesic motion at constant potential energy; because this dynamics is equivalent to Newtonian dynamics in the thermodynamic limit, the approximate invariance of the constant-potential-energy hypersurface implies virtually the same structure and dynamics of energy polydisperse LJ systems as for the single-component version. In contrast, the constant-potential-energy hypersurface is shown to be significantly affected by the introduction of size polydispersity.

* dyre@ruc.dk

I. INTRODUCTION

The term polydispersity is typically used for models characterized by a continuous distribution of parameters in the interaction potentials. This is relevant for describing the jamming of granular media, e.g., sand, which can be modeled by introducing a distribution of particle *sizes* [1–10]. Polydispersity is also relevant in the modeling of glass-forming liquids by allowing for fast equilibration via swap dynamics [11].

Size polydispersity is typically introduced via a distribution of the size parameter of the pair potential. If the "size" of particle i is σ_i, the Lorentz-Berthelot mixing rule states that the interaction with particle j involves the length parameter $(\sigma_i + \sigma_j)/2$ [12]. While size polydispersity is most commonly studied [1, 2, 4, 6–9, 13–18], a few publications have investigated the effects of energy polydispersity [19–22]. Using the Lorentz-Berthelot mixing rule for energies [12], Refs. 19 and 21 studied energy-polydisperse Lennard-Jones (LJ) fluids in 2d and found only very small differences at a given thermodynamic state point between the average properties of polydisperse systems and those of the single-component LJ fluid with the same average interaction energy. This was recently confirmed in a study of 3d energy-polydisperse LJ mixtures, demonstrating virtually invariant structure and dynamics when varying the degree of polydispersity [22]. Energy-polydispersity invariance is robust; thus Ref. 22 demonstrated that, except for the case of extreme energy polydispersity, the invariance property is maintained when varying the state point, the mixing rule, the energy probability distribution, or the pair potential. The question we address in this paper is: Why does the introduction of energy polydispersity not affect the structure and dynamics to any significant degree?

Before proceeding we note that the above-mentioned findings are consistent with the prediction of the so-called conformal solution theory [23] based on the idea that a mixture may be represented by a single-component liquid [24, 25]. This does not work well for size polydispersity, however [26]. According to the van der Waals mixing rule of conformal solution theory, the energy parameter of the one-component fluid representing the mixture is the average of the ij particle interaction energies $\langle \varepsilon_{ij} \rangle$. For the box distribution of particle energies ε_i studied in Ref. 22 this results in an average close to that obtained from the Lorentz-Berthelot mixing rule (and identical if one uses a linear energy-mixing rule, which also leads to invariant physics [22]).

In order to throw light on the energy-polydispersity invariance of structure and dynamics this paper adopts an NVU point of view. NVU dynamics replaces Newton's second law by Newton's first law – the law of inertia – by considering geodesic motion on the constant-potential-energy hypersurface in $3N$ dimensions where N is the number of particles [27, 28]. In the thermodynamic limit ($N \to \infty$) this gives rise to a time evolution that result in the same structure and dynamics as standard Newtonian dynamics [27, 28]. In fact, when NVU dynamics is discretized for numerical implementation, this leads to the leap-frog algorithm with a varying time step the relative fluctuations of which go to zero for $N \to \infty$ [28]. The conjecture investigated in this paper is that energy-polydisperse LJ mixtures have approximately the same constant-potential-energy hypersurfaces as those of the single-component LJ system. If validated, this would explain the observed invariance of structure and dynamics upon the introduction of energy polydispersity.

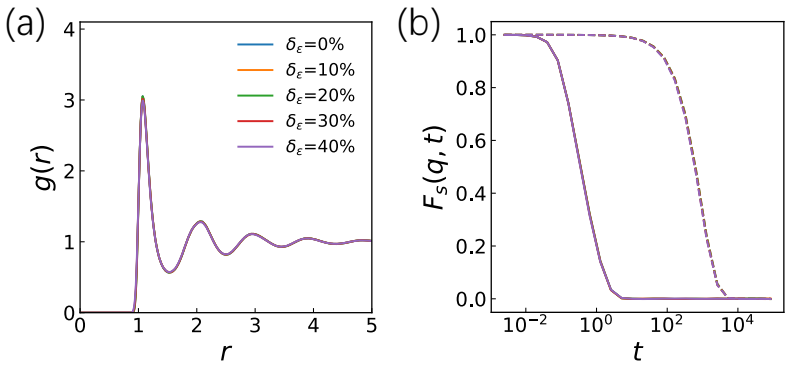

FIG. 1. Average structure and dynamics of LJ systems of different energy polydispersity at the state point $(\rho, T) = (0.85, 0.70)$, which is close to the triple point of the single-component LJ system. (a) shows the average radial distribution function (RDF), $g(r)$, for polydispersities up to 40%. (b) shows the average incoherent intermediate scattering function, $F_s(q, t)$, where the solid lines represent data for the wave vector of the first peak of the static structure factor of the monodisperse system ($q = 7.2$) while the dashed lines represent data for the wave vector corresponding to the box length ($q = 0.19$). For both structure and dynamics we find results that are virtually independent of the degree of polydispersity. These findings confirm those of Ref. 22.

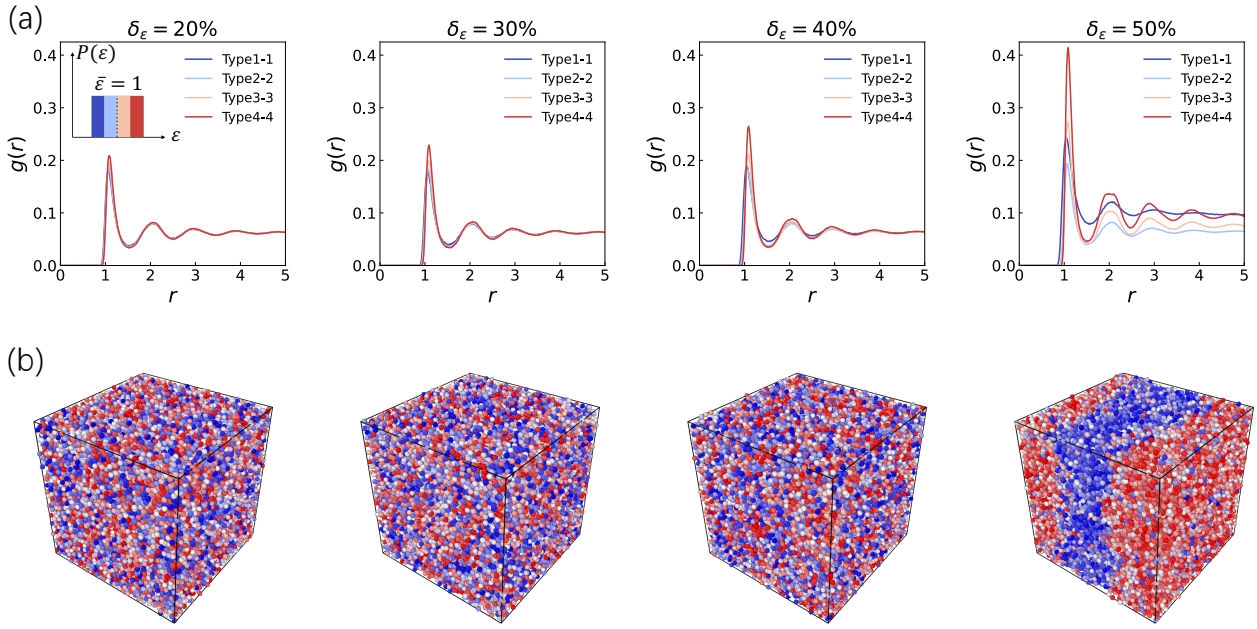

FIG. 2. Structure of LJ systems with energy polydispersity varying between 20% and 50% as quantified via the RDF. (a) For each polydispersity the particles are divided into four categories according to their energy as illustrated in the inset of the first panel. With increasing polydispersity the energy-resolved RDFs increasingly differ. (b) shows snapshots for each polydispersity in which the red particles have large energy and the blue have small energy.

II. APPROXIMATE INVARIANCE OF STRUCTURE AND DYNAMICS

This section sets the stage by detailing the systems studied and how they were simulated, giving results for the structure and dynamics confirming those of Ref. 22. We simulated energy-polydisperse Lennard-Jones (LJ) liquids in the NVT ensemble using "rumdpy" [29], an in-development Python version of the "Roskilde University Molecular Dynamics" (RUMD) GPU Molecular Dynamics software [30]. The LJ pair potential between two particles at distance r, $v(r)$, is given by

$$v(r) = 4\varepsilon \left((r/\sigma)^{-12} - (r/\sigma)^{-6} \right) . \tag{1}$$

Here ε is a characteristic energy and σ a characteristic distance (the "particle size"). For polydisperse systems these parameters vary between different particle pairs, usually according to a continuous probability distribution. This paper focuses on energy polydispersity. Thus σ is the same for all particles (and set to unity), whereas the characteristic energy of pair interaction ij follows the Lorentz-Berthelot mixing rule [12] and is given by $\varepsilon_{ij} = \sqrt{\varepsilon_i \varepsilon_j}$ where each particle has been assigned an energy ε_i chosen randomly from a box distribution centered around unity; in practice we operated with 256 different particle energies. The energy polydispersity δ_ε is defined as the standard deviation over the mean of this distribution, which in the case of mean energy equal to unity becomes $\delta_\varepsilon \equiv \sqrt{\langle \varepsilon^2 \rangle - 1}$.

Systems of $N = 32000$ particles of mass unity were simulated with standard Nose-Hoover NVT dynamics at the state point $(\rho, T) = (0.85, 0.70)$, which is close to the triple point of the single-component LJ system. This is the state point studied throughout. The time step used was 0.0025 (in LJ units used henceforth where $\varepsilon = \sigma = 1$ in Eq. (1)). A standard shifted-potential cutoff at 2.5 was used, but we also simulated the same systems with a shifted-force cutoff at 1.5 [31], leading to virtually identical results for the structure and dynamics (Appendix).

Figure 1 shows the structure and dynamics for the energy polydispersities δ_ε = 0%; 10%; 20%; 30%; 40%. The first case corresponds to the single-component LJ system; the next four correspond to particle energies varying between 0.83 and 1.17 (10% polydispersity), between 0.65 and 1.35 (20% polydispersity), between 0.48 and 1.52 (30% polydispersity), and between 0.31 and 1.69 (40% polydispersity) (the case of 50% polydispersity studied in Fig. 2 corresponds to particle energies varying between 0.13 and 1.87). These are quite significant polydispersities. Nevertheless, the average radial distribution function (RDF), $g(r)$, (Fig. 1(a)) and the average incoherent intermediate scattering function, $F_s(q,t)$, (Fig. 1(b)) are virtually the same for all five systems.

To which degree the neighborhood of a given particle correlates with its energy is analyzed in Fig. 2 for polydisper-

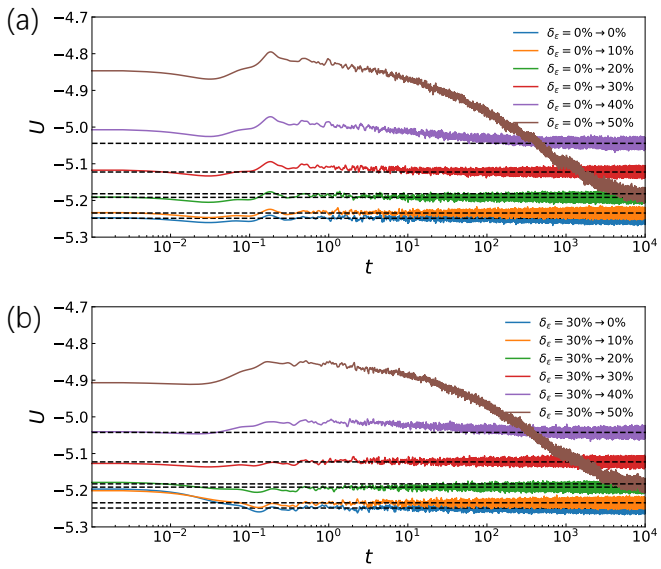

FIG. 3. Potential-energy relaxation after an instantaneous change of energy polydispersity. (a) Jumping from the equilibrium single-component system to different polydispersities. (b) Jumping from the equilibrium 30% polydispersity system to different polydispersities. In most cases little happens. This is consistent with the assumption that the system is in equilibrium immediately after the degree of polydispersity was changed, which is as expected if the constant-potential-energy hypersurface is invariant. For jumps to 50% polydispersity this is not the case, however, and the data confirm the phase separation observed as this system eventually is equilibrated (Fig. 2(b)). For the jumps to 40% polydispersity there is a slight tendency of a similar behavior.

sities going up to 50%. For each polydispersity we divided the particles into four categories according to their energy, each of which contains one quarter of the particles (inset). Figure 2(a) shows that as the polydispersity is increased, the energy-resolved RDFs increasingly differ, i.e., the neighborhood of each particle depends more and more on its energy. As shown in Fig. 2(b), the case of 50% polydispersity self-organizes by continuously phase separating into high (red) and low (blue) energy particles [22].

To investigate this effect further, we study in Fig. 3 how the potential energy relaxes toward equilibrium after polydispersity is introduced at $t = 0$. The idea is that if there is phase separation deriving from self-organization, the energy will relax slowly toward its equilibrium value. Figure 3(a) shows the time evolution of the average potential energy per particle, U, after jumps at $t = 0$ from the single-component system to polydispersities up to 50%, while (b) shows similar data for jumps starting from 30% polydispersity. In both cases the jumps to and from 30% polydispersity and below equilibrate quickly, while jumps to 50% polydispersity show a slow relaxation toward equilibrium. This confirms that self-organization takes place in the latter case. The jumps to 40% show a slight hint of the same behavior. Hence we leave out the two highest energy polydispersities (40% and 50%) from the below analysis.

III. DIGRESSION: NVU DYNAMICS IN BRIEF

This section briefly reviews NVU dynamics [27, 28, 32–34], which is an alternative molecular dynamics characterized by strict conservation of the potential energy (which does not apply, of course, for Newtonian dynamics). For systems of many particles, these two dynamics lead to the same structure and dynamics; this is because in the thermodynamic limit of Newtonian dynamics the *relative* fluctuations of the potential energy U go to zero. This has been shown theoretically and numerically for both atomic [27, 28] and molecular [32] models.

Consider a system of N particles in three dimensions with periodic boundary conditions. It is convenient to introduce the $3N$-dimensional configuration vector $\mathbf{R} \equiv (\mathbf{r}_1, ..., \mathbf{r}_N)$ in which $\mathbf{r}_i$ is the position of particle i. A constant-potential-energy hypersurface Ω is defined by the value of the potential energy U_0,

$$\Omega = \{\mathbf{R} \,|\, U(\mathbf{R}) = U_0\} \,. \tag{2}$$

Equation (2) defines a $3N - 1$ dimensional so-called level surface, which in this case is a submanifold of the $3N$ dimensional torus of all particle positions corresponding to periodic boundary conditions. The hypersurface Ω has

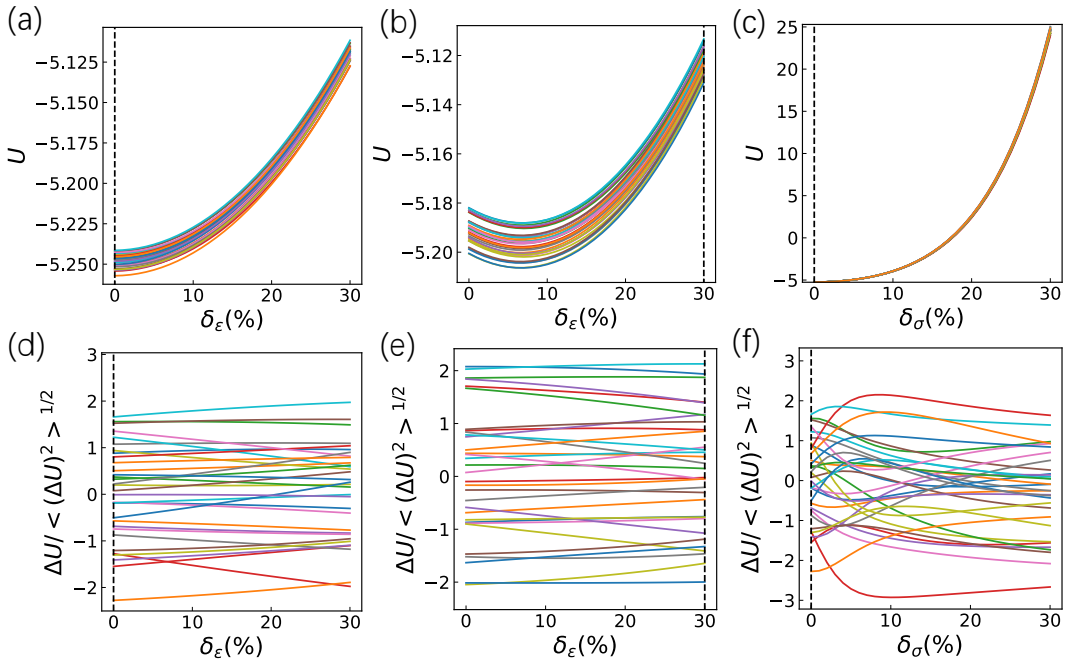

FIG. 4. Potential energies of configurations as a function of the degree of energy polydispersity. (a) and (b) show the potential energies of 32 independent configurations taken from an equilibrium simulation at 0% and 30% energy polydispersity, respectively. Once the configurations have been selected (marked by the vertical dashed line), the degree of polydispersity is changed in the expression for U (i.e., no further simulations are carried out). A closer look at the crossings is provided in (d) and (e) that show the relative potential-energy variations of the data of (a) and (b). The observed rare crossings mean that energy polydisperse LJ systems to a good approximation conform to Eq. (3), which is equivalent to having invariant Ω. For comparison, (c) and (f) show the effect of introducing size polydispersity.

the metric inherited from Euclidean space and is thereby a Riemannian manifold. This makes it possible to define *geodesics* as curves of minimum length or, more accurately, of stationary length in the sense that the length does not change for small curve perturbations keeping endpoints fixed. NVU dynamics is defined as geodesic motion on Ω [27]. This motion proceeds with constant velocity, so both the potential and the kinetic energy is conserved in NVU dynamics. In physical terms, NVU dynamics may be thought of as embodying friction-less motion on a curved surface in high dimensions, i.e., as expressing the law of inertia for motion on the curved hypersurface Ω.

It follows that systems with identical constant-potential-energy hypersurfaces have the same structure and dynamics, also for standard Newtonian dynamics. This fact motivated us to investigate whether the Ω hypersurfaces change only little when energy polydispersity is introduced, which would offer a simple rationalization of the observed invariance of the physics after introducing even sizable energy polydispersity.

IV. APPROXIMATE INVARIANCE OF THE CONSTANT-POTENTIAL-ENERGY HYPERSURFACES

Returning to the invariance of structure and dynamics when energy polydispersity is introduced, the observations of Fig. 1 would, as mentioned above, be explained if the constant-potential-energy hypersurfaces Ω are independent – or almost independent – of the energy polydispersity. We proceed to investigate whether this is the case. Note first, however, that there is no theoretical reason a given Ω is completely unaffected by the degree of energy polydispersity. Thus any two configurations, which have identical potential energy at one polydispersity, will most likely have different potential energies for another polydispersity. This means that checking invariance of the identity $U(\mathbf{R}_\mathrm{a}) = U(\mathbf{R}_\mathrm{b})$ is not a useful way to investigate the potential (approximate) invariance of the constant-potential-energy hypersurface. Instead, we take inspiration from isomorph theory that considers invariance of the inequality $U(\mathbf{R}_\mathrm{a}) < U(\mathbf{R}_\mathrm{b})$ under changing conditions (in that case when configurations are scaled uniformly). Specifically, comparing two potential-energy functions corresponding to different energy polydispersities, $U_1(\mathbf{R}) \equiv U(\mathbf{R}, \delta_\varepsilon^{(1)})$ and $U_2(\mathbf{R}) \equiv U(\mathbf{R}, \delta_\varepsilon^{(2)})$, we wish to investigate numerically how well the following logical implication is obeyed

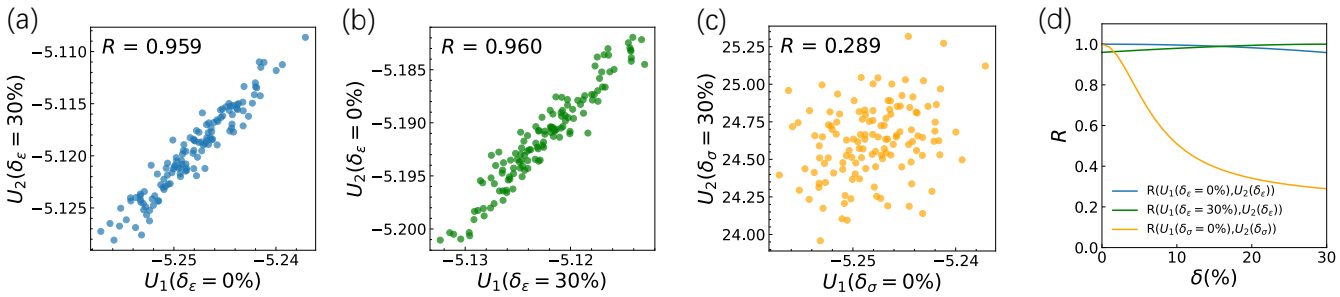

FIG. 5. Correlation coefficient R between the potential energy of configurations sampled from the equilibrium state of the potential U_1 corresponding to some polydispersity, subsequently evaluated with respect to a different polydispersity resulting in the potential energy U_2. (a) Correlation between the single-component system, U_1, and 30% energy polydispersity, U_2. (b) The reverse of (a); configurations were here selected from a 30% energy polydispersity simulation and subsequently evaluated with respect to zero polydispersity. The strong correlations observed in (a) and (b) stand in contrast to what happens for size polydispersity; thus (c) shows the analogous correlation between the potential energies of the single-component system and that of 30% size polydispersity. Finally, (d) shows how R varies as a function of polydispersity for the two cases of energy polydispersity (blue and green, corresponding to (a) and (b), respectively) and size polydispersity (yellow). Note that in the latter case the correlation drops quickly.

$$U_1(\mathbf{R}_\mathrm{a}) < U_1(\mathbf{R}_\mathrm{b}) \implies U_2(\mathbf{R}_\mathrm{a}) < U_2(\mathbf{R}_\mathrm{b})\,. \tag{3}$$

If this were to apply rigorously for all configurations, one could conclude that $U_1(\mathbf{R}_\mathrm{a}) = U_1(\mathbf{R}_\mathrm{b}) \implies U_2(\mathbf{R}_\mathrm{a}) = U_2(\mathbf{R}_\mathrm{b})$, i.e., that system 1 and 2 have the exactly same Ωs. If one more realistically observes that Eq. (3) applies for most configurations though not always, the corresponding constant-potential-energy hypersurfaces are not identical, merely almost identical. In the latter case, by reference to NVU dynamics one expects approximately invariant structure and dynamics.

To check Eq. (3) numerically we proceeded as follows. We sampled several configurations from an equilibrium simulation of system 1, e.g., the single-component LJ system. The configurations were sampled at times separated enough that they were statistically independent. For each configuration, we then evaluated the potential energy corresponding to a different degree of polydispersity and monitored how this quantity changed, i.e., no further MD simulations were carried out. Plotting these potential energies as a function of the polydispersity yields a figure confirming Eq. (3) if none of the curves cross each other (Ref. 35 did this first by uniformly scaling configurations to test for the hidden scale invariance that forms the basis of isomorph theory).

Figure 4(a) shows such a plot in which the configurations were selected from an equilibrium simulation of the single-component system, while (b) shows the analog if configurations are selected from an equilibrium simulation at 30% energy polydispersity (in which case the new polydispersities were obtained by a uniform scaling of the energies relative to unity). The first thing one notices is that the value of the potential energy changes only a little. Moreover, there are only few curve crossings, which to a significant degree validates Eq. (3). Figures 4(d) and (e) study the crossings in more detail by plotting the relative variation of the potential energy as a function of the degree of polydispersity, i.e., after the average of U has been subtracted and the data subsequently normalized to unit variance. In all panels, the vertical dashed lines mark the polydispersity of the system simulated to generate the configurations.

For comparison, Figure 4(c) shows the same when size polydispersity is introduced. While for energy polydispersity, there are only few crossings, and when two curves do cross they generally stay close, neither of these observations apply for size polydispersity. A further conclusion is that there is little difference between selecting the configurations from the single-component LJ system and then introducing polydispersity, (a) and (c), and selecting the configurations at 30% energy polydispersity and subsequently removing entirely the polydispersity, (b) and (d). This confirms that the configurations remain equilibrium configurations to a good approximation after changing the polydispersity (which in fact follows from the approximate invariance of Ω).

Figure 4 features several instances of "weak" crossings in the sense that the two potential energies stay close even if they cross at some energy polydispersity. Intuitively, one expects this must imply a less severe violation of the proposed invariance of Ω than if, e.g., the energies vary wildly as in the case of size polydispersity, Fig. 4(f). How to quantify this? A simple possibility is to calculate how the Pearson correlation coefficient between the initial and final potential energies, U_1 and U_2, vary. Figure 5(a) shows a plot of the $\delta_\varepsilon = 0$ data of Fig. 4(a) versus its δ_ε =30% data, and Fig. 5(b) shows the reverse correlation plot. In both cases there is a strong correlation (note that this plot involves

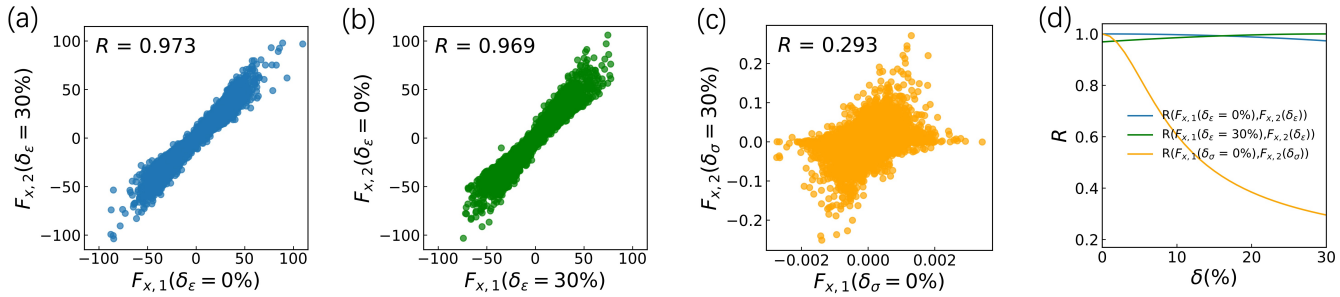

FIG. 6. Correlation between the individual particle forces in the x-direction, F_x, of a single configuration sampled from the equilibrium state of some polydispersity, subsequently evaluated with respect to a different polydispersity. (a) Correlation between the single-component system and 30% energy polydispersity. (b) The reverse of (a); configurations were here equilibrated at 30% energy polydispersity $\delta_\epsilon = 0.3$ and the forces were subsequently evaluated with respect to 0% polydispersity. In both cases there is a strong correlation. This is in contrast to what happens in the case of size polydispersity; thus (c) shows R between the single-component system and 30% size polydispersity, while (d) shows how R varies as a function of polydispersity for the two cases of energy polydispersity (blue and green, respectively corresponding to (a) and (b)) and size polydispersity (yellow). In the latter case the correlation drops quickly.

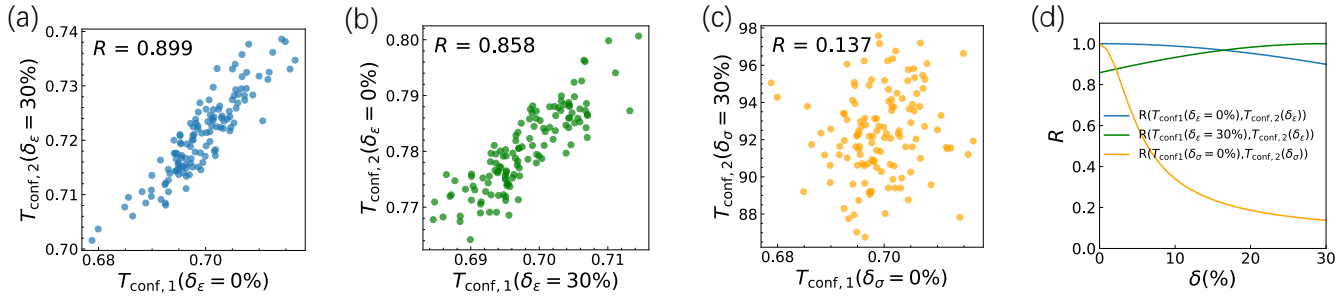

FIG. 7. Correlation between the configurational temperatures T_{conf} of configurations sampled from the equilibrium state of some polydispersity and T_{conf} evaluated with respect to a different polydispersity. (a) Correlation between the single-component system and 30% energy polydispersity. (b) The reverse of (a); configurations were here equilibrated at 30% energy polydispersity and the configurational temperatures subsequently evaluated with respect to 0% polydispersity. In both cases there is a strong correlation, which is in contrast to what happens in the case of size polydispersity. Thus (c) shows R between the single-component system and 30% size polydispersity, while (d) shows how R varies as a function of polydispersity for the two cases of energy polydispersity (blue and green, respectively corresponding to (a) and (b)) and size polydispersity (yellow). In the latter case the correlation drops quickly.

many more configurations than the 32 of Fig. 4). We take this as a quantitative confirmation of the conjecture that energy polydispersity leads to only minor modifications of the constant-potential-energy hypersurfaces.

It is instructive to compare to size polydispersity. This is studied in an analogous way in Fig. 5(c) for the data of Fig. 4(f) starting from the monodisperse LJ system. This time there is a very poor correlation between the original $\delta_\sigma = 0\%$ polydispersity and $\delta_\sigma = 30\%$ polydispersity. In fact, the correlation coefficient drops quickly as a function of polydispersity, as is clear from Fig. 5(d) that shows the correlation coefficients as a function of polydispersity for all three cases.

V. TWO FURTHER APPROXIMATE INVARIANTS

The $3N$-dimensional collective force vector composed of all particle forces is minus the gradient of $U(\mathbf{R})$. Two systems with identical Ω at any given state point will have proportional collective force vectors (normal to Ω), but not necessarily of same length. A closer analysis, which will not be repeated here, shows that the macroscopic so-called *reduced* force vectors [36] are identical, however, leading to the same structure and dynamics even though the temperatures may differ for two systems at two state points with the same Ω [33, 34]. In the present case of energy polydispersity with energies that average to unity, there is no need to adjust the temperature, however. Thus one way to confirm the above finding of closely similar Ωs when changing the energy polydispersity is to look at the

distribution of the individual particle forces [22].

We carried out such an analysis with a focus on calculating the Pearson correlation coefficient, again changing between 0% and 30% polydispersity. Figure 6(a) shows a scatter plot of the x-coordinates of all particle forces in the former case, while (b) shows the reverse change. We find in both cases a strong correlation. The linear-regression slopes are close to, though not equal to, unity. This suggests that a slight adjustment of the temperature would result in even better collapse of the RDFs and of the intermediate scattering functions (Fig. 1), but this effect will be minor and we did not investigate it further. For comparison, we show in Fig. 6(c) the same analysis when going from the single-component system to 30% size polydispersity. In this case the forces correlate only weakly, and as shown in (d) a significant "decorrelation" takes effect even when just a minor size polydispersity is introduced (yellow curve).

That the temperatures corresponding to a given Ω are virtually independent of the energy polydispersity can be validated by considering the so-called configurational temperature $T_{\rm conf}$, a quantity that refers exclusively to the configurational degrees of freedom [34, 37–40]. The configurational temperature is a property of Ω with the convenient property that $T_{\rm conf} = T$ for a system in thermal equilibrium, i.e., for a configuration that is "typical" of Ω. $T_{\rm conf}$ is defined as a ratio of two canonical averages, $k_B T_{\rm conf} \equiv \langle (\nabla U)^2 \rangle / \langle \nabla^2 U \rangle$. For a large system $T_{\rm conf}$ can be reliably evaluated from a single equilibrium configuration because the relative fluctuations of both terms go to zero.

Figure 7 shows plots analogous to those of Fig. 6 with $T_{\rm conf}$ instead of the individual x-components of the particle forces. Note that while the latter gives many data points for each configuration, the former yields just a single point, meaning that several configurations are needed to make the plot, just as for U in Fig. 5. The results, however, are quite similar to those of Fig. 6: Going from 0% to 30% energy polydispersity or the reverse, the configurational temperatures correlate strongly, which is not the case when size polydispersity is considered.

VI. SUMMARY

We have shown that the constant-potential-energy hypersurfaces of energy polydisperse LJ systems are virtually independent of the degree of polydispersity in the range 0%-30% and therefore almost identical to those of the single-component LJ system. By reference to NVU dynamics, this explains why structure and dynamics are not affected by energy polydispersity to any significant degree. This is different from what happens when size polydispersity is introduced, in which case the constant-potential-energy hypersurfaces are not invariant and both structure and dynamics change dramatically [22]. – It would be nice to have analytical arguments for the approximate Ω invariance when energy polydispersity is introduced, a challenge we leave for future considerations.

[1] E. Dickinson, "Equations of state of polydisperse hard-disc and hard-sphere systems," Chem. Phys. Lett. **57**, 148 (1978).
[2] J. J. Salacuse and G. Stell, "Polydisperse systems: Statistical thermodynamics, with applications to several models including hard and permeable spheres," J. Chem. Phys. **77**, 3714 (1982).
[3] D. Frenkel, R. J. Vos, C. G. de Kruif, and A. Vrij, "Structure factors of polydisperse systems of hard spheres: A comparison of monte carlo simulations and percus-yevick theory," J. Chem. Phys. **84**, 4625 (1986).
[4] R. M. L. Evans, "Fractionation of polydisperse systems: Multiphase coexistence," Phys. Rev. E **59**, 3192 (1999).
[5] E. R. Weeks, J. C. Crocker, A. C. Levitt, A. Schofield, and D. A. Weitz, "Three-dimensional direct imaging of structural relaxation near the colloidal glass transition," Science **287**, 627 (2000).
[6] M. Fasolo and P. Sollich, "Equilibrium phase behavior of polydisperse hard spheres," Phys. Rev. Lett. **91**, 068301 (2003).
[7] S. E. Abraham, S. M. Bhattacharrya, and B. Bagchi, "Energy landscape, antiplasticization, and polydispersity induced crossover of heterogeneity in supercooled polydisperse liquids," Phys. Rev. Lett. **100**, 167801 (2008).
[8] P. Ballesta, A. Duri, and L. Cipelletti, "Unexpected drop of dynamical heterogeneities in colloidal suspensions approaching the jamming transition," Nat. Phys. **4**, 550 (2008).
[9] D.-H. Nguyen, E. Azéma, F. Radjai, and P. Sornay, "Effect of size polydispersity versus particle shape in dense granular media," Phys. Rev. E **90**, 012202 (2014).
[10] T. S. Ingebrigtsen and H. Tanaka, "Effect of size polydispersity on the nature of Lennard-Jones liquids," J. Phys. Chem. B **119**, 11052–11062 (2015).
[11] A. Ninarello, L. Berthier, and D. Coslovich, "Models and algorithms for the next generation of glass transition studies," Phys. Rev. X **7**, 021039 (2017).
[12] M. P. Allen and D. J. Tildesley, Computer Simulation of Liquids (Oxford Science Publications (Oxford), 1987).
[13] J. A. Gualtieri, J. M. Kincaid, and G. Morrison, "Phase equilibria in polydisperse fluids," J. Chem. Phys. **77**, 521 (1982).
[14] D. A. Kofke and E. D. Glandt, "Monte carlo simulation of continuous lennard-jones mixtures," FFE **29**, 327 (1986).
[15] S. Auer and D. Frenkel, "Suppression of crystal nucleation in polydisperse colloids due to increase of the surface free energy," Nature **413**, 711 (2001).

[16] N. B. Wilding and P. Sollich, "Liquid-vapour phase behaviour of a polydisperse lennard-jones fluid," J. Phys.: Condens. Matter **17**, S3245 (2005).

[17] W. M. Jacobs and D. Frenkel, "Predicting phase behavior in multicomponent mixtures," J. Chem. Phys. **139**, 024108 (2013).

[18] S. Sarkar, R. Biswas, M. Santra, and B. Bagchi, "Solid-liquid transition in polydisperse lennard-jones systems," Phys. Rev. E **88**, 022104 (2013).

[19] L. S. Shagolsem and Y. Rabin, "Particle dynamics in fluids with random interactions," J. Chem. Phys. **144**, 194504 (2016).

[20] T. S. Ingebrigtsen and H. Tanaka, "Effect of energy polydispersity on the nature of Lennard-Jones liquids," J. Phys. Chem. B **120**, 7704–7713 (2016).

[21] L. S. Shagolsem and Y. Rabin, "Particle dynamics in fluids with random interactions," J. Chem. Phys. **144**, 194504 (2016).

[22] T. S. Ingebrigtsen and J. C Dyre, "Even strong energy polydispersity does not affect the average structure and dynamics of simple liquids," J. Phys. Chem. B **127**, 2837–2846 (2023).

[23] K. E. Gubbins, "The theory of non-electrolyte solutions: an historical review," Mol. Phys. **111**, 3666–3697 (2013).

[24] G. A. Mansoori, "Radial distribution functions and their role in modeling of mixtures behavior," Fluid Phase Equilib. **87**, 1–22 (1993).

[25] M. S. Shell, P. G. Debenedetti, and A. Z. Panagiotopoulos, "A conformal solution theory for the energy landscape and glass transition of mixtures," Fluid Phase Equilib. **241**, 147 (2006).

[26] M. J. Pond, J. R. Errington, and T. M. Truskett, "Implications of the effective one-component analysis of pair correlations in colloidal fluids with polydispersity," J. Chem. Phys. **135**, 124513 (2011).

[27] T. S. Ingebrigtsen, S. Toxvaerd, O. J. Heilmann, T. B. Schrøder, and J. C. Dyre, "NVU dynamics. I. Geodesic motion on the constant-potential-energy hypersurface," J. Chem. Phys. **135**, 104101 (2011).

[28] T. S. Ingebrigtsen, S. Toxvaerd, T. B. Schrøder, and J. C. Dyre, "NVU dynamics. II. Comparing to four other dynamics," J. Chem. Phys. **135**, 104102 (2011).

[29] "The rumdpy package can be found at https://gitlab.com/tbs.cph/rumdpy-dev," (2024).

[30] N. P. Bailey, T. S. Ingebrigtsen, J. S. Hansen, A. A. Veldhorst, L. Bøhling, C. A. Lemarchand, A. E. Olsen, A. K. Bacher, L. Costigliola, U. R. Pedersen, H. Larsen, J. C. Dyre, and T. B. Schrøder, "RUMD: A general purpose molecular dynamics package optimized to utilize GPU hardware down to a few thousand particles," Scipost Phys. **3**, 038 (2017).

[31] S. Toxvaerd and J. C. Dyre, "Communication: Shifted forces in molecular dynamics," J. Chem. Phys. **134**, 081102 (2011).

[32] T. S. Ingebrigtsen and J. C. Dyre, "NVU dynamics. III. Simulating molecules," J. Chem. Phys. **137**, 244101 (2012).

[33] J. C. Dyre, "NVU Perspective on Simple Liquids' Quasiuniversality," Phys. Rev. E **87**, 022106 (2013).

[34] J. C. Dyre, "Isomorphs, Hidden Scale Invariance, and Quasiuniversality," Phys. Rev. E **88**, 042139 (2013).

[35] T. B. Schrøder and J. C. Dyre, "Simplicity of condensed matter at its core: Generic definition of a Roskilde-simple system," J. Chem. Phys. **141**, 204502 (2014).

[36] N. Gnan, T. B. Schrøder, U. R. Pedersen, N. P. Bailey, and J. C. Dyre, "Pressure-energy correlations in liquids. IV. "Isomorphs" in liquid phase diagrams," J. Chem. Phys. **131**, 234504 (2009).

[37] L. D. Landau and E. M. Lifshitz, Statistical Physics [Eq. (33.14)] (Pergamon, Oxford, 1958).

[38] H. H. Rugh, "Dynamical approach to temperature," Phys. Rev. Lett. **78**, 772–774 (1997).

[39] J. G. Powles, G. Rickayzen, and D. M. Heyes, "Temperatures: old, new and middle aged," Mol. Phys. **103**, 1361–1373 (2005).

[40] S. Saw, L. Costigliola, and J. C. Dyre, "Configurational temperature in active matter. I. Lines of invariant physics in the phase diagram of the Ornstein-Uhlenbeck model," Phys. Rev. E **107**, 024609 (2023).

APPENDIX

We here present results corresponding to those of the main paper using instead a shifted-force cutoff. This cutoff is defined by modifying the pair force below the cutoff radius by adding a constant ensuring that the pair force at the cutoff radius is zero [31]. In NVE simulations, this results in a much better energy conservation than a shifted-potential cutoff. It has been demonstrated for the single-component LJ system that a shifted-force cutoff at just 1.5 is enough to obtain as accurate results as those of a shifted-potential cutoff at 2.5 [31]; this is the case even although the LJ pair force is 30 times larger at distance 1.5 than at distance 2.5. This fact allows for a speed up of simulations of a factor of four.

This Appendix repeats the analysis of the main paper, using a shifted-force cutoff at 1.5. The overall findings of the main paper are confirmed and no new conclusions are arrived at.

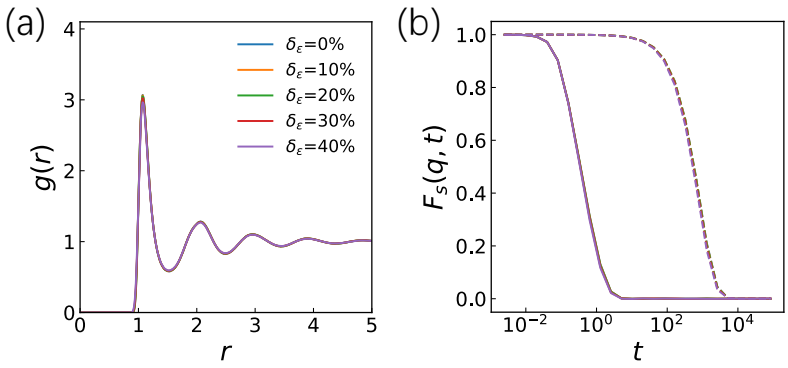

FIG. A1. Average structure and dynamic of LJ systems of different energy polydispersity simulated with a shifted-force cutoff at 1.5 at the state point $(\rho, T) = (0.85, 0.70)$. This figure is the shifted-force analog of Fig. 1. (a) shows the average RDF for polydispersities up to 40%. (b) shows the average incoherent intermediate scattering function where solid lines represent the wave vector of the first peak of the static structure factor of the single-component LJ system ($q = 7.2$) and dashed lines represent the wave vector corresponding to the box length ($q = 0.19$). For both structure and dynamics, as in Fig. 1 we find results that are virtually independent of the degree of polydispersity.

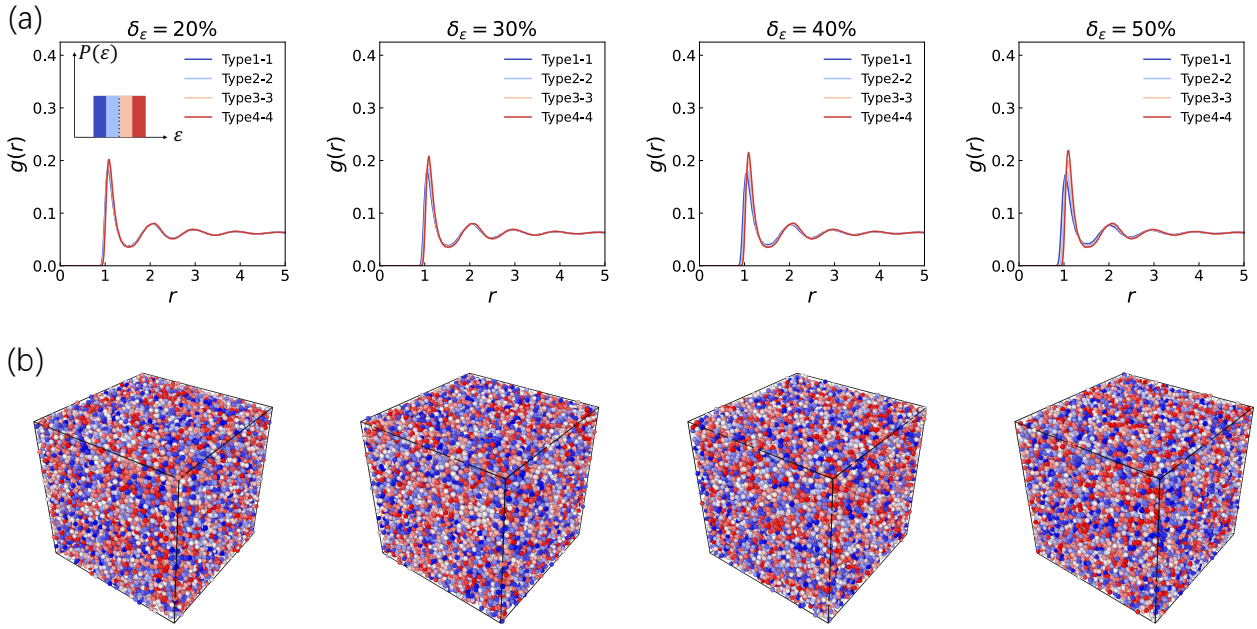

FIG. A2. Structure of LJ systems with energy polydispersity varying between 20% and 50% simulated with a shifted-force cutoff at 1.5 at the state point $(\rho, T) = (0.85, 0.70)$. This figure is the shifted-force analog of Fig. 2. (a) The particles are divided into four categories according to their energy as illustrated in the inset of the first panel. With increasing polydispersity these energy-resolved RDFs differ more and more. Interestingly, the difference is less pronounced than for the shifted-potential simulations of the main paper. (b) shows snapshots for each polydispersity in which the red particles have large energy and the blue have small energy. In contrast to the findings of the main paper, there is no clearly visible phase separation at the highest polydispersity.

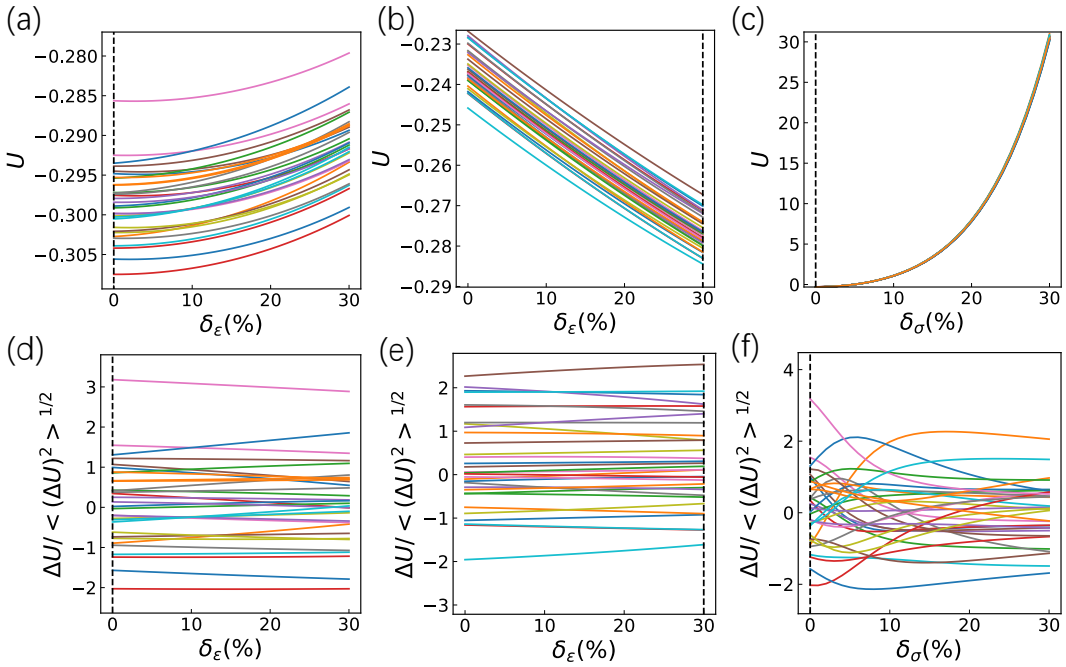

FIG. A3. Potential energies of configurations as a function of the degree of polydispersity. This figure is the shifted-force analog of Fig. 4. Note that the potential energy used here differs from that of the main paper (reflecting the fact that the pair forces are modified below the cutoff). (a) and (b) show the potential energies of 32 independent configurations taken from an equilibrium simulation at 0% and 30% energy polydispersity, respectively. A closer look at the crossings is provided in (d) and (e) that show the relative potential-energy variations of the data in (a) and (b). The observed rare crossings mean that energy polydisperse LJ systems to a good approximation conform to Eq. (3), which is equivalent to having invariant Ω. For comparison, (c) and (f) show the effect of introducing size polydispersity.

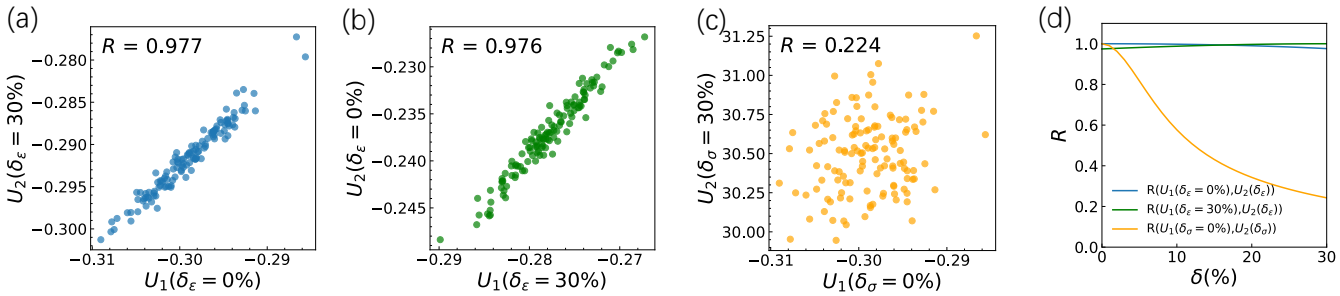

FIG. A4. Correlation between the potential energy of configurations sampled from the equilibrium state of the potential U_1 corresponding to some polydispersity, subsequently evaluated with respect to a different polydispersity resulting in the potential energy U_2. This figure is the shifted-force analog of Fig. 5. (a) R between the single-component system, U_1, and 30% energy polydispersity, U_2. (b) The reverse of (a); configurations were here equilibrated at 30% energy polydispersity and subsequently evaluated with respect to zero polydispersity. In both cases there is a strong correlation. The strong correlations observed in (a) and (b) stand in contrast to what happens in the case of size polydispersity for which (c) shows R between the single-component system 30% size polydispersity. Finally, (d) shows how R varies as a function of polydispersity for the two cases of energy polydispersity (blue and green) and size polydispersity (yellow). In the latter case the correlation drops quickly.

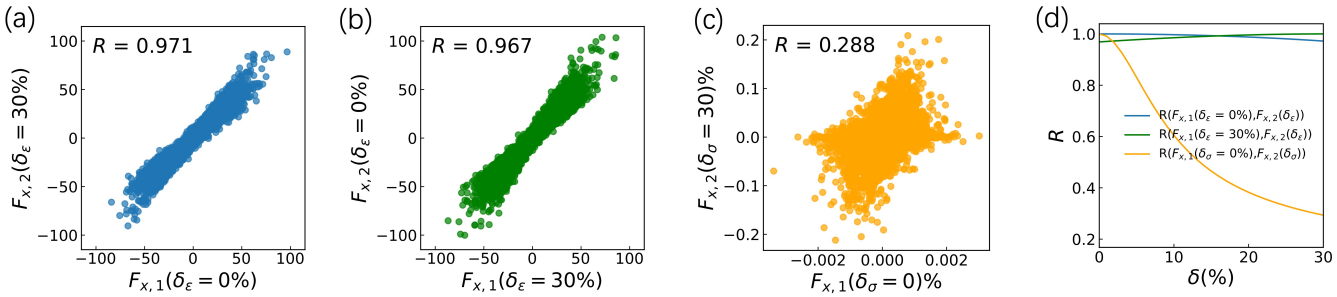

FIG. A5. Correlation between the individual particle forces in the x-direction, F_x, of a single configuration sampled from the equilibrium state of some polydispersity, subsequently evaluated with respect to a different polydispersity. This figure is the shifted-force analog of Fig. 6. (a) Correlation between the single-component system and 30% energy polydispersity. (b) The reverse of (a); the configuration is here an equilibrium configuration at 30% energy polydispersity and the forces were subsequently evaluated with respect to 0% polydispersity. In both cases there is a strong correlation, which is in contrast to what happens in the case of size polydispersity; thus (c) shows the correlation between the single-component system and 30% size polydispersity. Finally, (d) shows how R varies as a function of polydispersity for the two cases of energy polydispersity (blue and green) and size polydispersity (yellow). In the latter case the correlation drops quickly.

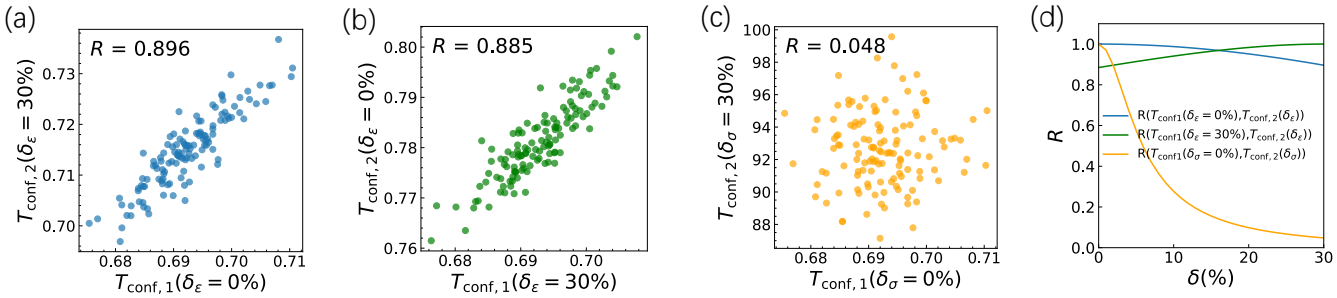

FIG. A6. Correlation between the configurational temperatures T_{conf} of configurations sampled from the equilibrium state of some polydispersity and the configurational temperature evaluated with respect to a different polydispersity. This figure is the shifted-force analog of Fig. 7. (a) Correlation between the single-component system and 30% energy polydispersity. (b) The reverse of (a); configurations were here equilibrated at 30% energy polydispersity and the configurational temperatures subsequently evaluated with respect to 0% polydispersity. In both cases there is a strong correlation, which is in contrast to what happens in the case of size polydispersity. Thus (c) shows the correlation between the single-component system and 30% size polydispersity. Finally, (d) shows how R varies as a function of polydispersity for the two cases of energy polydispersity (blue and green) and size polydispersity (yellow). In the latter case the correlation drops quickly.